STRUCTURAL SCIENCE
CRYSTAL ENGINEERING
MATERIALS

ISSN: 2052-5206
journals.iucr.org/b

A crystallographic and thermal study of pridinol mesylate and its monohydrated solvate

Pablo Gaztañaga, Ricardo Baggio and Daniel Roberto Vega

Acta Cryst. (2018). B**74**, 304–310

STRUCTURAL SCIENCE
CRYSTAL ENGINEERING
MATERIALS

ISSN 2052-5206

A crystallographic and thermal study of pridinol mesylate and its monohydrated solvate

Pablo Gaztañaga,[a,b,c]* Ricardo Baggio[a] and Daniel Roberto Vega[a,b]

[a]Gerencia de Investigación y Aplicaciones, Centro Atómico Constituyentes, Comisión Nacional de Energía Atómica, Av. Gral Paz 1499, San Martin, Buenos Aires B1650KNA, Argentina, [b]Escuela de Ciencia y Tecnología, Universidad Nacional General San Martín, Martín de Irigoyen 3100, San Martín, Buenos Aires CP 1650, Argentina, and [c]CONICET (Consejo Nacional de Investigaciones Científica y Técnicas), Argentina. *Correspondence e-mail: pablogzt@gmail.com

Received 23 March 2018
Accepted 8 May 2018

Edited by J. Lipkowski, Polish Academy of Sciences, Poland

Keywords: active pharmaceutical ingredient; pridinol mesylate; crystal structure; hydrates; rate-dependent dehydration.

CCDC references: 1842103; 1842104

Supporting information: this article has supporting information at journals.iucr.org/b

Herein are reported the crystal and molecular structures of the pridinol mesylate salt ($C_{20}H_{25}NO^{+}\cdot CH_3O_3S^{-}$) (I) and its monohydrated solvate form ($C_{20}H_{25}NO^{+}\cdot CH_3O_3S^{-}\cdot H_2O$) (II). A comparison of both with the already reported structure of pure pridinol [1,1-diphenyl-3-piperidino-1-propanol, $C_{20}H_{25}NO$; Tacke *et al.* (1980). *Chem. Ber.* **113**, 1962–1980] is made. Molecular structures (I) and (II) are alike in bond distances and bond angles, but differ in their spatial conformation, and, more relevant still, in their hydrogen-bonding motifs. This gives rise to quite different packing schemes, in the form of simple dimers in (I) but water-mediated hydrogen-bonded chains in (II). The dehydration behaviour of form (II) is highly dependent on the heating rate, with slow rates leading to a clear endothermic dehydration step, towards anhydrous (I), with subsequent melting of this latter phase. Increased heating rates result in a more unclear behaviour ending in a structural collapse (melting of the hydrated phase), at temperatures significantly lower than the melting point of the anhydrous phase. The eventual relevance of the water link in the structure of (II) is discussed in regard to this behaviour.

1. Introduction

Pridinol [1,1-diphenyl-3-piperidino-1-propanol, $C_{20}H_{25}NO$, (III)] is a centrally-acting muscle relaxant and it is usually administrated in the form of its mesylate salt. Its weakening action on polysynaptic reflexes occurs predominantly on the spinal motor neurons, where pridinol mesylate inhibits the propagation of the stimulus transmitted by the receptor. Because of this, the muscle tone decreases in the resting state, but the ability of spontaneous muscle contraction is not affected. The drug also presents favourable pharmacokinetic properties: after intramuscular or oral administration, pridinol mesylate is absorbed very quickly in animal tests, where after 30–40 min the maximum level in blood is achieved. The drug is indicated in the relaxing treatment of muscle contractures of the musculoskeletal system, both of central origin (as in the case of cerebral vascular diseases, tremors due to Parkinson's disease, diseases or spinal cord injuries, *etc.*) and peripheral (as in the case of osteoarthritis, for example lumbosacral, herniated intervertebral disc, low-back pain, flat feet, sciatica, torticollis, muscular pains in general, night cramps, *etc.*).

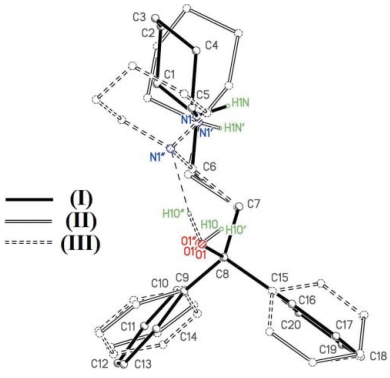

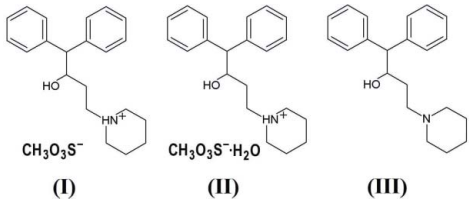

Table 1
Crystallographic and refinement details.

	(I)	(II)	(III)†
Crystal data			
Chemical formula	$C_{21}H_{29}NO_4S$	$C_{21}H_{31}NO_5S$	$C_{20}H_{25}NO$
M_r	391.51	409.53	295.4
Crystal system, space group	Monoclinic, $P2_1/c$	Monoclinic, $P2_1/n$	Monoclinic, $P2_1/c$
Temperature (K)	295	295	n.a.
a, b, c (Å)	8.7198 (2), 20.996 (8), 10.9186 (3)	8.2086 (2), 17.9355 (6), 15.0983 (5)	5.859 (2), 15.798 (5), 18.029 (7)
β (°)	94.357 (2)	94.770 (2)	90.31 (6)
V (Å^3)	1993.2 (8)	2215.15 (12)	1668.75
Z	4	4	4
D (g cm^{-3})	1.305	1.228	1.18
Radiation, wavelength (Å)	Mo $K\alpha$, 0.71073	Mo $K\alpha$, 0.71073	Cu $K\alpha$, 1.54178
μ (mm^{-1})	0.19	0.18	4.8
Data collection			
No. of measured, independent and observed reflections	8157, 4393, 3300 [$I > 2\sigma(I)$]	9717, 4896, 3559 [$I > 2\sigma(I)$]	n.a., n.a., 2189 [$I > 1.5\sigma(I)$]
R_{int}	0.018	0.022	n.a.
$(\sin\theta/\lambda)_{max}$ (Å^{-1})	0.666	0.667	n.a.
Refinement			
$R[F^2 > 2\sigma(F^2)]$, $wR(F^2)$, S	0.045, 0.117, 1.04	0.051, 0.133, 1.03	0.07, n.a., n.a.
No. of reflections	4393	4896	2189
No. of parameters	252	261	299
No. of restraints	0	3	n.a.
$\Delta\rho_{max}$, $\Delta\rho_{min}$ (e Å^{-3})	0.29, −0.31	0.33, −0.30	n.a., n.a.

Computer programs: *CrysAlis PRO* (Oxford Diffraction, 2009), *SHELXS97* (Sheldrick, 2008), *SHELXL97*, *SHELXL2014* (Sheldrick, 2015*b*), *SHELXTL* (Sheldrick, 2015*a*), *PLATON* (Spek, 2009). † Reported by Tacke *et al.* (1980). n.a: information not available.

On the other hand, when an API (active pharmaceutical ingredient), such as pridinol mesylate, is manufactured, the final crystallization process must assure that the desired solid form is obtained in a consistent, pure and reproducible manner. Subsequently, when the compound is formulated, in particular during wet granulation, knowledge about potential hydrates (or solvates in general) is especially useful. In the case of hydrates, several studies have shown that phase transformations and mixtures of solid-state forms can occur during wet processes (Wikström *et al.*, 2005; Williams *et al.*, 2004; Gift *et al.*, 2009; Petrova *et al.*, 2009). Moreover, in some attempts to reverse hydrate formation, the drying process can lead either to a form different to the original API (Phadnis & Suryanarayanan, 1997; Dugué *et al.*, 1991) or even to the formation of a different material, after dehydration (Saleki-Herhardt *et al.*, 1995; Li *et al.*, 2000). It is clear then that the existence of different phases has an immediate impact in any manufacturing process and their physicochemical characterization is relevant for knowledge about the stability of the different phases.

Even if an extensive bibliography can be found regarding therapeutic properties of pridinol and its mesylate salt, covering a large time interval (see Giordani *et al.*, 1985; Fassina *et al.*, 1986; Luo *et al.*, 2014, 2015, *etc.*), there is scarce information on the structural details: only a single-crystal study of the free base (III) could be traced in the literature (Tacke *et al.*, 1980). As as a contribution to alleviate this lack of information, we present here a crystal and molecular study of two mesylate salts, namely, the anhydrous one [$C_{20}H_{25}NO{\cdot}CH_3O_3S$, (I)] and its monohydrated solvatomorph [the form in which it is pharmacologically administrated, $C_{20}H_{25}NO{\cdot}CH_3O_3S{\cdot}H_2O$, (II)], as well as a detailed analysis of the dehydration process linking them, including some physicochemical characterization looking for the clarification of the thermal stability of both forms. In addition, a structural comparison with the already reported free base (III) is performed.

2. Experimental

2.1. Crystallization

Pridinol mesylate (in its hydrated form) was kindly provided by Laboratorios Raffo, Argentina. Crystals of the anhydrous phase (I) were obtained by slow solidification of the melt and those for the monohydrated phase (II) from recrystallization of a water solution, even if it was observed that similar results were obtained from almost any solvent bearing some water contamination.

2.2. Instrumental techniques

Thermogravimetric studies were performed with a Shimadzu DTG-50 apparatus, while a TA instrument (model Q2000) was used for differential scanning calorimetry (DSC). In both cases, the experiments were carried out under an N_2 atmosphere, with a 10 ml min^{-1} flux. Room-temperature single-crystal data for for (I) and (II) were collected on an Oxford Gemini A CCD diffractometer using Mo $K\alpha$ radiation (λ = 0.71073 Å) and XRPD diagrams obtained in a Panalytical Empyrean diffractometer with Cu $K\alpha$ radiation (λ = 1.54178 Å). The dehydration process was also followed optically using a Carl Zeiss Axioskop 40 microscope, coupled to an

Table 2
Selected bond distances (Å) and torsion angles (°).

	(I)	(II)	(III)
Bond distances			
N1—C1	1.499 (3)	1.500 (2)	1.4684 (6)
N1—C5	1.491 (3)	1.497 (3)	1.4686 (6)
N1—C6	1.498 (3)	1.494 (2)	1.4655 (6)
Torsion angles			
N1—C6—C7—C8	129.81 (18)	174.87 (15)	62.0
C6—C7—C8—O1	−63.3 (2)	−59.0 (2)	−56.3
C6—C7—C8—C9	54.3 (2)	58.27 (19)	65.7
C6—C7—C8—C15	173.84 (16)	−179.19 (15)	−173.8
O1—C8—C9—C10	143.99 (17)	174.59 (16)	−172.7
C7—C8—C9—C10	24.7 (2)	56.4 (2)	65.6
C15—C8—C9—C10	−96.6 (2)	−67.5 (2)	−56.7
O1—C8—C15—C16	−3.4 (2)	45.3 (2)	47.0
C7—C8—C15—C16	117.43 (19)	165.47 (17)	166.5
C9—C8—C15—C16	−118.68 (19)	−71.5 (2)	−71.4

INSTEC HCS302 hot/cold stage, a STC200 temperature controller, and a Nikon DS camera.

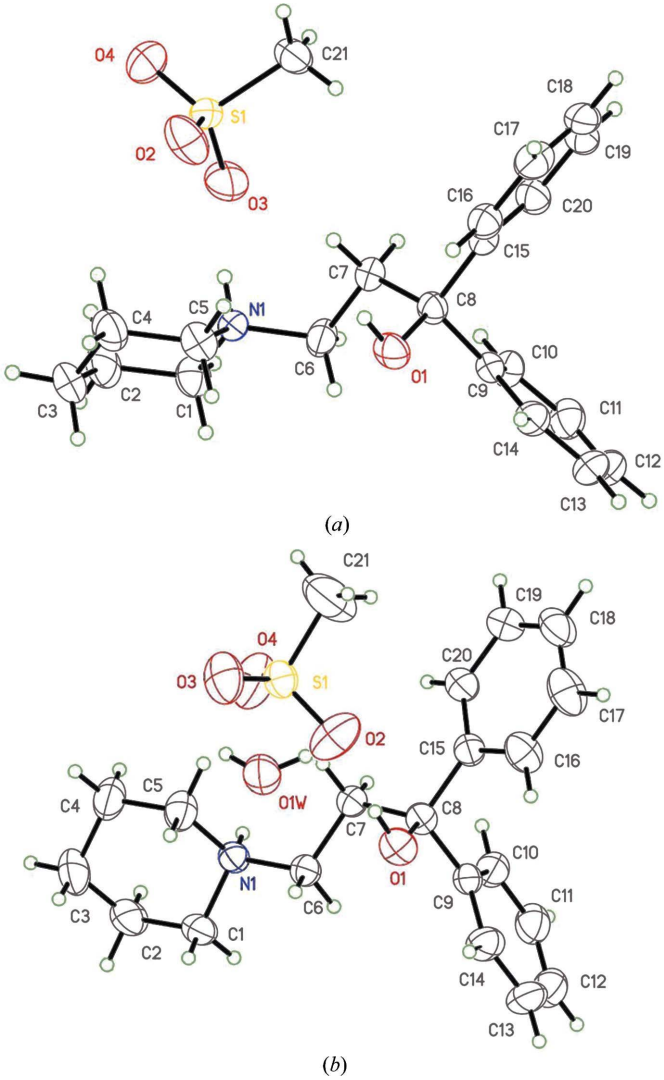

Figure 1
Molecular representations of (*a*) (I) and (*b*) (II). Displacement ellipsoids drawn at the 40% level probability level.

Table 3
Hydrogen-bonding interactions (Å, °).

No.	*D*—H···*A*	*D*—H	H···*A*	*D*···*A*	*D*—H···*A*
(I)					
#1	O1—H1O···O2^{i}	0.82 (3)	2.20 (3)	3.006 (3)	167 (3)
#2	N1—H1N···O3	0.86 (2)	2.18 (2)	2.948 (2)	149.1 (18)
#3	N1—H1N···O2	0.86 (2)	2.48 (2)	3.249 (2)	150.0 (18)
#4	C5—H5*C*···O2^{i}	0.97	2.45	3.407 (3)	171
#5	C1—H1*C*···O4^{ii}	0.97	2.57	3.504 (3)	161
(II)					
#1	O1—H1O···O2	0.845 (19)	1.913 (18)	2.745 (2)	167.9 (19)
#2	N1—H1N···O1*W*	0.856 (15)	1.874 (16)	2.728 (2)	175.6 (16)
#3	O1*W*—H1*WA*···O3^{iii}	0.853 (18)	1.882 (18)	2.732 (2)	174 (2)
#4	O1*W*—H1*WB*···O4^{iv}	0.851 (12)	1.886 (11)	2.734 (2)	174 (2)
#5	C7—H7*A*···O4	0.97	2.52	3.476 (2)	168
#6	C17—H17···O1*w*^{v}	0.93	2.59	3.458 (3)	156
(III)					
#1	O1—H1O···N1	0.82	2.05	2.7383 (11)	141

Symmetry codes: (i) $-x+1, -y+1, -z+1$; (ii) $x+1, y, z$; (iii) $x-1, y, z$; (iv) $-x+1, -y+2, -z+1$; (v) $\frac{1}{2}+x, \frac{3}{2}-y, -\frac{1}{2}+z$.

2.3. Refinement

All H atoms were originally found in difference Fourier maps, but treated differently in refinement. The H atoms bonded to O and N were refined with restrained O—H = N—H = 0.85 (1) Å, U(H) = 1.2U_{equiv}(host), while H atoms bonded to C were repositioned in their expected positions and allowed to ride with U(H) = xU_{eq}(C) [d(C—H$_{arom}$) = 0.93 Å, x = 1.2; d(C—H$_{methylene}$) = 0.97 Å, x = 1.2; d(C—H$_{methyl}$) = 0.96 Å, x = 1.5].

3. Results and discussion

3.1. Crystal and molecular structure

Fig. 1 shows ellipsoid plots of (I) and (II), while Table 1 presents some relevant crystallographic data. Those corresponding values for structure (III) have also been included, for comparison purposes, and the same applies to Table 2 (some relevant distances and torsion angles) and Table 3 (hydrogen-bonding interactions). The most noticeable difference between the neutral moiety (III) and the cationic ones in (I) and (II) resides in the piperidine N in the former one being replaced by a piperidinium NH^{+} in the mesylate salts. This H atom plays a significant role in the packing scheme of (I) and (II), but its existence also shows up in a relaxation of the C—N distances in the piperidinium ring, as compared with the piperidine one, with a lengthening of ∼2% (Table 2).

Apart of these differences all three structures are metrically equivalent, and the only perceivable differences are to be found in the selected torsion angles shown in Table 2, describing movements with respect to the central C8-O1-C7-C9-C15 backbone. This is better grasped graphically in Fig. 2, which shows a superposition of this rigid group in the three structures. Again, a clear difference arises from the absence of the NH^{+} group in (III), which allows for the approach of the OH group to the piperidine ring, leading to a strong intramolecular OH···N bond. The effect can be observed in Fig. 2 through the rotation of the O—H bond from the locus of the

remaining two, as well as the strong deviation of the piperidine ring.

The remaining differences can be ascribed to the diversity of packing demands in the crystal structures; for instance, those derived from the unhampered rotations of the phenyl rings around C8—C9 and C8—C15. Regarding these latter rotations, structures (II) and (III) present similar values (Table 2), while structure (I) differs significantly.

The most relevant hydrogen-bonding interactions are presented in Table 3. Those for structure (III) reduce to the single OH···N intramolecular bond already discussed, whose effect is to give the molecule a 'closed' appearance, and to isolate it from its environment (at least in what strong interactions regards) because no relevant donors or acceptors remain available. This fact is reflected in the rather low density of the compound (1.18 g cm^{-3}).

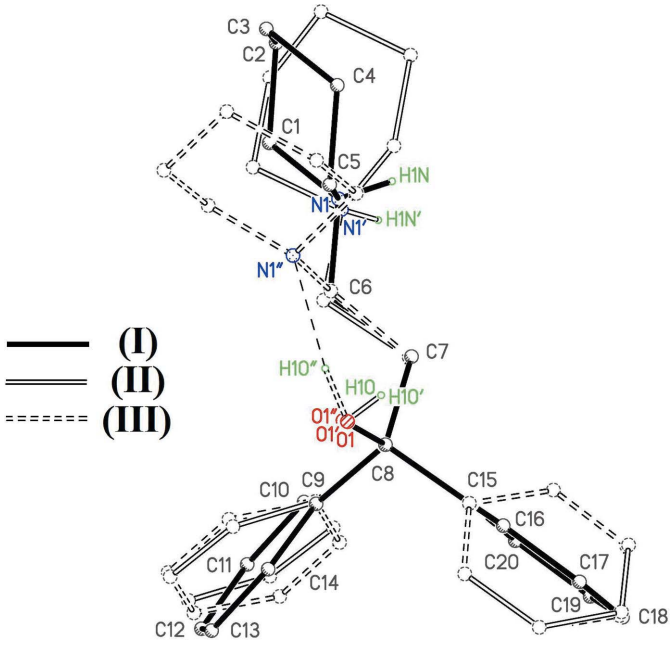

Figure 2
Superposition of (I), (II) and (III) having the C8-O1-C7-C9-C15 backbone as the matching sequence. Unprimed atoms refer to (I), singly primed (′) to (II) and doubly primed (″) to (III).

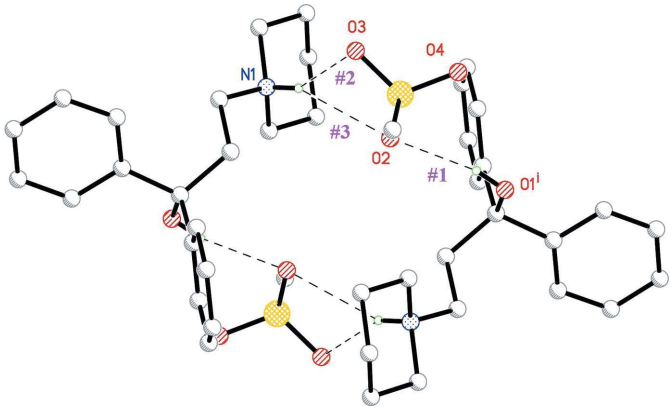

Figure 3
Dimeric unit in (I). Hydrogen bonds are indicated by broken lines, and labelled as in Table 3.

Second in complexity ranks structure (I), with the mesylate acceptor acting as a link for the formation of a centrosymmetric dimer (Fig. 3 and Table 3).

The presence of the water molecule in (II) allows for a more complex crystal structure. The main motif here is a one-dimensional structure running along [100], where a centrosymmetric $R_4^4(16)$ (mesylate·H_2O)$_2$ loop (Fig. 4) acts as a linker between centrosymmetric pairs of pridinol molecules, which are not bound to each other but to the linker *via* hydrogen bonds #1 and #2 (Table 3). In all cases there are second-order C—H···O bonds completing the intermolecular interactions.

3.2. The (II)–(I) dehydration process and the kinetic problem

When structure (II) is subjected to a low-rate heating process (< 1°C min^{-1}; Fig. 5, upper curve), it dehydrates with a broad endothermic event (range 80–100°C) fully converting into the anhydrous (I), as confirmed by the neat melting at *ca* 162°C, characteristic of the crystalline, nonhydrated solvatomorph. The same was observed when the dehydration process was performed on bulky samples, allowing for the product identification by XRPD.

If left unperturbed at environmental conditions, the anhydrous phase slowly incorporates water, indicating it is metastable in nature. The process is greatly enhanced when performed in a water-saturated environment, as shown in Fig. 6, which displays the temporal evolution, presented as the complementary percentage of (I) and (II) when samples initially consisting of pure phase (I) are subjected to these extreme conditions, during different periods of time. In ∼4 h, the process seems to stabilize at a 80–20% (II)–(I) ratio.

Solid curves in Fig. 6 represent an exponential fitting of the experimental data, which discloses a reaction speed constant

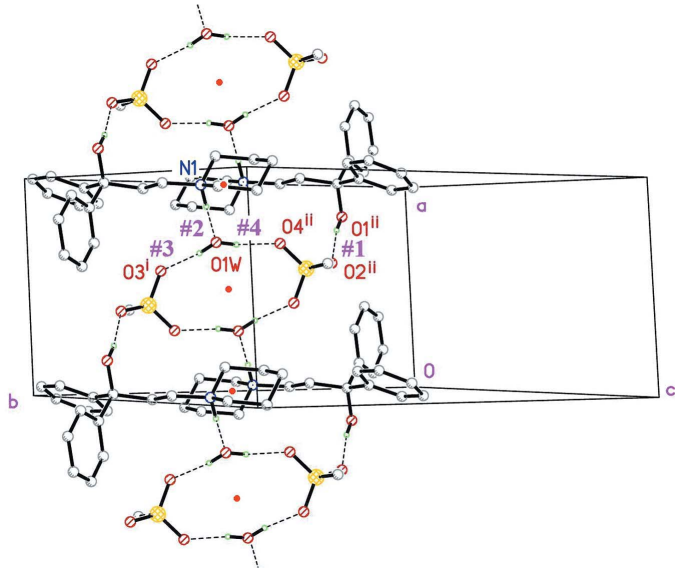

Figure 4
One-dimensional structure of (III). Hydrogen bonds are shown dashed lines, and labelled as in Table 3. The red dots represent inversion centres.

k = 0.027 (1) min^{-1} (valid just for these humidity and temperature conditions).

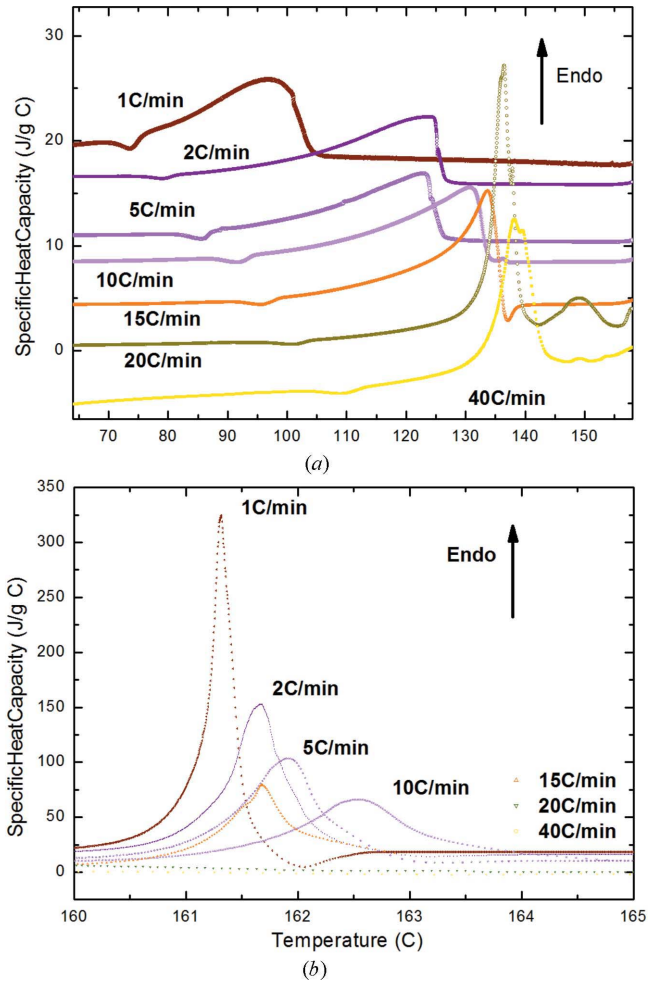

Figure 5
DSC patterns run at different heating rates, showing (*a*) the dehydration process of (II) (event A) and (*b*) the later fusion endotherm of (I) (event B) generated in the process.

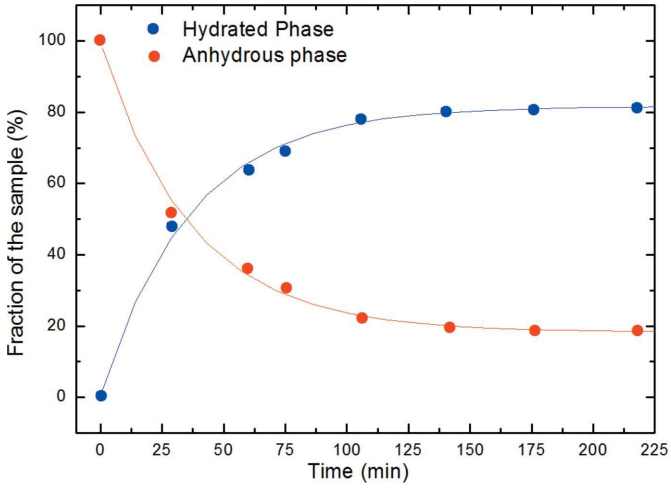

Figure 6
Concentration curves of both phases, (I) and (II), when an initial sample of (II) was in a highly humid environment, for different periods of time.

The percentages of each phase at different hydration times were determined by the Rietveld refinement of the corresponding XRPD diagrams. Fig. S1 in the supporting information shows a couple of examples of these refinements, clearly disclosing the kind of agreement achieved.

What has been described so far could be considered as 'classic' results in the expected manner.

However, when the dehydration of (II) is followed by a set of DSC runs at different heating rates (Fig. 5), some unusual results were obtained. All diagrams are characterized by two events, which for clarity we shall call A (lower temperature) and B (higher temperature).

Event A is rather complex to analyse, with an irregular shape ascribable to a main endothermic component plus a number of concomitant secondary processes which defy a clear explanation (namely, the small exothermal peak systematically appearing at slightly lower temperatures, *etc.*). The second event, B, is also endothermic but much sharper and ascribable to melting of the crystalline anhydrate. The most significant details in Fig. 5 are summarized as follows:

(*a*) In the first run (1°C min^{-1}) event A appears as rather broad [and clearly assignable to dehydration of the monohydrate in a solid → solid, (II) → (I) transformation] and the second (B) much sharper and associated to melting of the resulting crystalline anhydrate.

(*b*) On increasing the heating rate, the temperature at which event B occurs is unchanged, within a ±1°C range, while decreasing significantly in the associated enthalpy. In other words, there is a significant decrease in the mass of the originally hydrated material (II) which transforms into the crystalline anhydrate (I).

The broad endotherm at *ca* 80°C already described for heating rate 1°C min^{-1}, as corresponding to a pure (II) → (I) dehydration, moves significantly towards higher temperatures and gets sharper, gradually resembling much more the peak for a melting process than for a pure solid → solid dehydration. In parallel, optical observation of the different processes discloses some partial melting at these intermediate stages.

(*c*) Increasing the heating rate still further leads to a stage (around 20°C min^{-1}) where event B disappears altogether (or at least becomes undetectable), event A becoming extremely sharp and the single one in the process. When checked under a polarizing microscope, this event is seen to correspond to a complete melting of the analysed sample.

3.3. A 'first-order approximation' model

As already commented, the process is rather difficult to explain in detail, mainly due to the complexity of event A. On the other hand, this should not be much of a surprise, the process under study being a 'far from equilibrium' one.

There are, however, some conclusions which may be drawn by correlating the crystal structure of both compounds and the results described in §3.2.

The structural changes required to go from the hydrated structure (II) to the anhydrous (I) (upper curve in Fig. 5) are simply explained with the help of Figs. 3, 4 and 7.

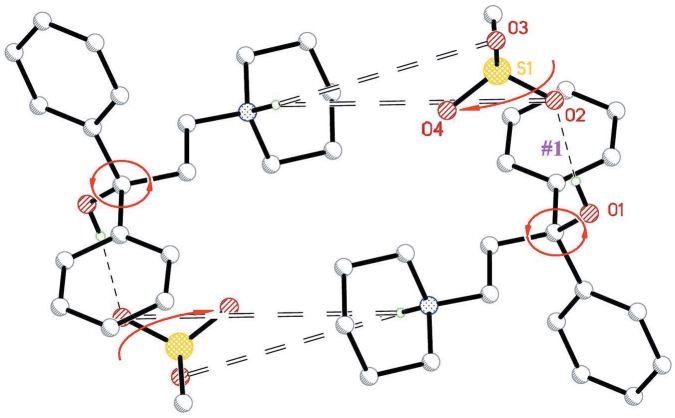

Figure 7
Sketch of an eventual transient state in (II) after losing the water molecule. Red arrows indicate the molecular movements required to bring the (non-interacting) distances in double dashed lines into the (interacting) N—H···O ones drawn in simple dashed lines in Fig. 3 (#2 and #3). Single dashed lines indicate, in the present figure, the same O—H··· bond (#1) as in Fig. 3.

When the water solvate in (II) is removed, the link in the chain breaks (see Fig. 4), leaving as nearest neighbours the two pridinol and two mesylates shown in Fig. 7. The similarity of this disposition with the dimer in (I) (Fig. 3) is apparent. Only slight rotations/displacements of the molecules (suggested by the red arrows in Fig. 7) are required to bring the non-interacting distances (shown as double dashed lines in Fig. 7) into the interacting ones in the (I) dimer (single dashed lines in Fig. 3).

Thus, if the process is driven in a rather slow fashion, the structure has the ability to accommodate to the new situation and the crystalline anhydrous phase (I) results as the only outcome.

However, as the heating rate increases, this re-accommodation process appears to be gradually impeded, with only a fraction of the 'water-free' material being able to reach the 'ordered' state (I), the rest being unable to cope and collapsing in the way of melting of the hydrated phase (II). The complexity of event A, with its line narrowing and peak shift, has to do with the superposition of both processes, the melting peak giving the group an asymmetric profile and apparently dragging the composite to higher temperatures. Only in a few snapshots (with large crystals samples) could we serendipitously catch both events as separated ones. See peaks A and A′ in Fig. S2 (supporting information).

As the heating rate increases further, both results (namely, the decrease of the (II) → (I) dehydration peak and the increase of the melted fraction) are enhanced, with this latter event being more relevant as suggested by the extremely sharp peak shape, finally stabilizing at $T \sim 135$°C.

The process has its climax at heating rate ∼20°C min^{-1}, and at ∼40°C min^{-1} almost all the available hydrate (II) melts, with no correlation for (I) being detectable.

However, it should be noted that this is only valid at extremely high heating rates. In the case of lower heating rates (*i.e.* 10°C min^{-1}), the situation at temperatures in the intermediate range between both melting points is as follows: some molten material [coming from the melt of (II)] coexists with dehydrated material in phase (I) [coming from the simultaneous (II) → (I) dehydration]. Since the temperature is lower than the melting point of (I), proper conditions for seeding and growth from the melt are set, and large crystals of (I) may develop. This is shown in Fig. 8, where four different steps in a 10°C min^{-1} run are shown, beginning at T = 100°C with an incipient melt of (II), followed by an advanced melting stage at 115°C, coexisting with with seeds of powdered (I). This results in a rapid crystal growth of (I) (snapshot at 150°C), to end up at 180°C with the complete melting of the whole system.

Figure 8
Micrographs of a heating sequence (run at a heating rate of 10°C min^{-1}) showing the dehydration process of (II) with further recrystallization from the melt of the anhydrous phase (I). (*a*) T = 100°C [beginning of (II) melt], (*b*) 115°C [advanced melt, coexisting with seeds of powdered (I)], (*c*) 150°C [advanced crystal growth of (I)], (*d*) 180°C [above melting point of (I): full melt].

3.4. Conclusions

We have herein reported an interesting case of a solid→ solid dehydration process coexisting with the simultaneous melting of the hydrated phase, a highly out-of-equilibrium process which strongly depends on the heating rate.

These unusual results are certainly of academic interest but they could also be applicable to industrial processes, for instance, where hydrated phases are dried at rather high temperatures, as often happens in the pharmaceutical industry; thus raising an alert on the need to chose an adequate heating rate if undesirable results are to be avoided.

References

Dugué, J., Céolin, R., Rouland, J. C. & Lepage, F. (1991). *Pharm. Acta Helv.* **66**, 307–310.
Fassina, A., Rubinacci, A. & Tessari, L. (1986). *Int. J. Clin. Pharmacol. Res.* **6**, 501–507.

Gift, A. D., Luner, P. E., Luedeman, L. & Taylor, L. S. (2009). *J. Pharm. Sci.* **98**, 4670–4683.
Giordani, L., Amore, M., Montanari, A., Berlinzani, L. & Gentili, C. (1985). *Am. J. Psychiatry*, **142**, 389–390.
Li, Y. H., Han, J., Zhang, G. G. Z., Grant, D. J. W. & Suryanarayanan, R. (2000). *Pharm. Dev. Technol.* **5**, 257–266.
Luo, L., Luo, M., Luo, Y. & Bourkaib, N. (2014). *Lat. Am. J. Pharm.* **33**, 1175–1181.
Luo, X., Luo, M., Tan, M., Deng, L., Liu, S., Zhong, H., Luo, L. & Luo, Y. (2015). *Lat. Am. J. Pharm.* **34**, 358–363.
Oxford Diffraction (2009). *CrysAlis PRO*. Oxford Diffraction Ltd, Yarnton, Oxfordshire, England.
Petrova, R. I., Peresypkin, A., Mortko, C. J., McKeown, A. E., Lee, J. & Williams, J. M. (2009). *J. Pharm. Sci.* **98**, 4111–4118.
Phadnis, N. V. & Suryanarayanan, R. (1997). *J. Pharm. Sci.* **84**, 318–323.
Saleki-Gerhardt, A., Stoweell, J. G., Byrn, S. R. & Zografi, G. (1995). *J. Pharm. Sci.* **84**, 318–323.
Sheldrick, G. M. (2008). *Acta Cryst.* A**64**, 112–122.
Sheldrick, G. M. (2015*a*). *Acta Cryst.* A**71**, 3–8.
Sheldrick, G. M. (2015*b*). *Acta Cryst.* C**71**, 3–8.
Spek, A. L. (2009). *Acta Cryst.* D**65**, 148–155.
Tacke, R., Strecker, M., Sheldrick, W. S., Ernst, L., Heeg, E., Berndt, B., Knapstein, C.-M. & Niedner, R. (1980). *Chem. Ber.* **113**, 1962–1980.
Wikström, H., Marsac, P. J. & Taylor, L. S. (2005). *J. Pharm. Sci.* **94**, 209–219.
Williams, A. C., Cooper, V. B., Thomas, L., Griffith, L. J., Petts, C. R. & Booth, S. W. (2004). *Int. J. Pharm.* **275**, 29–39.